J Nanostruct 16(3): 3558-3574, Summer 2026

RESEARCH PAPER

A New NH_2-MIL-88B(Fe) Enhanced Carbon Paste Sensor: Simultaneous Determination of Dopamine and Phenylalanine

Monir Ebrahimipure [1], *Mehdi Shabani-Nooshabadi* [1,2] *

[1] *Institute of Nano Science and Nano Technology, University of Kashan, Kashan, I.R. Iran*

[2] *Department of Analytical Chemistry, Faculty of Chemistry, University of Kashan, Kashan, I.R. Iran*

ARTICLE INFO

Article History:
Received 05 March 2026
Accepted 22 May 2026
Published 01 July 2026

Keywords:
Carbon paste electrode
Dopamine
Electrochemical determination
MOF
Phenylalanine

ABSTRACT

The precise monitoring of dopamine, a vital neurotransmitter involved in the regulation of mood, cognition, and motor control, is of great importance. In this context, carbon paste electrodes have attracted considerable attention due to their ease of preparation, cost-effectiveness, and ability to be modified for enhanced sensitivity and accuracy. In the present study, NH_2-MIL-88B(Fe) was synthesized and characterized using fourier transform infrared spectroscopy (FTIR), X-ray diffraction (XRD), and scanning electron microscope (SEM) analyses, and subsequently employed to modify a carbon paste electrochemical sensor for the detection of dopamine in human and pharmaceutical samples and in the presence of phenylalanine. The synergistic effect of the synthesized metal–organic framework (MOF) combined with graphite led to a remarkable improvement in sensor performance, providing a wide linear response range from 0.7–100 µM and 100–900 µM, with an exceptionally low detection limit of 0.18 µM for dopamine, indicative of the high performance of the optimized electrode. Kinetic analysis further revealed a transfer coefficient (α) of 0.8 and a diffusion coefficient (D) of 4.3×10^{-6} cm^2/s.

How to cite this article
Ebrahimipure M., Shabani-Nooshabadi M. A New NH_2-MIL-88B(Fe) Enhanced Carbon Paste Sensor: Simultaneous Determination of Dopamine and Phenylalanine. J Nanostruct, 2026; 16(3):3558-3574. DOI: 10.22052/JNS.2026.03.047

INTRODUCTION

Simultaneously determining multiple pharmaceutical compounds without a preconcentration step represents a major analytical challenge [1]. Dopamine, an essential neurotransmitter, requires precise quantification due to its fundamental physiological roles [2]. As a key neurotransmitter, dopamine was initially characterized in 1958 by Carlsson and his team at the Laboratory of Chemical Pharmacology of Sweden's National Heart Institute [2, 3]. Carlsson later received the Nobel Prize in Physiology or Medicine in 2000 for these foundational discoveries [4]. Neurotransmitters are generally categorized based on their effect on postsynaptic receptors, being either excitatory or inhibitory. Uniquely, dopamine exhibits both actions and holds vital importance within the central nervous, renal, cardiovascular, and endocrine systems [5, 6].

A deviation from normal dopamine concentrations is connected to various disorders. Excessively high levels may induce cardiotoxic effects, including tachycardia, hypertension, heart failure, and addictive behaviors. On the other hand, a deficit of this neurotransmitter correlates with conditions such as stress, Parkinson's disease (according to Hornykiewicz) [7, 8], schizophrenia [9], Alzheimer's disease [10, 11], and depression [12, 13]. Therefore, precise measurement of

* *Corresponding Author Email: m.shabani@kashanu.ac.ir*

dopamine is crucial for deciphering its functions in biological systems and the related neural signaling routes [14-16]. These pathological associations further underline the analytical demand for sensitive, reproducible, and reliable detection platforms capable of monitoring dopamine fluctuations under physiologically relevant conditions.

According to recent investigations employing analytical and epidemiological strategies beyond descriptive biochemical observation, dopamine concentration in the striatum has been reported to be inversely related to Parkinson's symptoms [17-19], highlighting the metabolic and clinical relevance of pathway-level interpretation. Approaches such as causal-inference modeling and clinically oriented metabolic assessment have further emphasized that phenylalanine participates in a broader physiological network linked to dopamine regulation rather than acting solely as a precursor. Increasing dopamine concentration is considered as a treatment for Parkinson's [20, 21]. For this purpose, the L-DOPA medication (3,4-dihydroxyl-phenylalanine, Levodopa), which is a dopamine precursor, L-DOPA is widely recognized as an effective therapeutic strategy [22, 23]. In dopaminergic neurons, dopamine is obtained from the precursor tyrosine, and phenylalanine plays a role in providing tyrosine. This synthesis pathway is in the form of phenylalanine-tyrosine-L-DOPA-dopamine conversion, which provides the dopamine needed by the brain. Thus, it can be concluded that phenylalanine can play a role in brain dopamine levels and Parkinson's disease. In addition, various studies have shown that phenylalanine deficiency can cause phenylketonuria, attention deficit hyperactivity disorder, schizophrenia, and adverse neurological outcomes [24, 25]. Taken together, this interconnected metabolic framework reinforces the analytical importance of investigating dopamine behavior in the presence of phenylalanine, particularly in studies aimed at developing sensing platforms capable of resolving closely related biochemical species.

The detection of dopamine has been accomplished through multiple analytical techniques. For instance, an Ultra-High-Performance Liquid Chromatography coupled with Electrospray Ionization Quadrupole Time-of-Flight Mass Spectrometry (UHPLC/ESI-Q-TOF-MS) method was established to quantify dopamine in Wistar rat brain tissue. In a comparable study, High-Performance Liquid Chromatography coupled with Tandem Mass Spectrometry (HPLC-MS/MS) was applied for analogous dopamine analysis. Despite their high sensitivity and reliability, these instrumental approaches often require expensive equipments, extensive sample preparation, and lack real-time applicability; therefore, ongoing research seeks alternative analytical strategies capable of overcoming these practical limitations [26, 27].

As a cost-efficient and comfortably available option, electrochemical methods present benefits including portability, user-friendliness, and considerable sensitivity [28]. Electrochemical sensing refers to analytical measurement based on monitoring electrical signals (current, potential, or impedance) generated by redox reactions at an electrode–solution interface, where achieving strong selectivity in the presence of interfering species remains a central design challenge. In this context, Khamlichi et al. developed an L-leucine-modified sol–gel carbon electrode for the voltammetric determination of homovanillic acid and dopamine in urine samples related to neuroblastoma diagnostics. Their approach demonstrated enhanced effective surface area, improved electrocatalytic activity, clear separation of oxidation peaks, and sub-micromolar detection capability, highlighting the potential of amino acid-based surface modification for boosting sensitivity and selectivity while maintaining simple electrode preparation and regeneration [29]. Subsequently, more sophisticated composite sensors incorporating stable and robust materials have been investigated, yet a significant number of these are still confined to operation in simplified buffer media instead of intricate biological samples [30].

Considerable researchs focus has been directed toward improving electrode functionality via modification with nanomaterials [31]. Metal–organic frameworks (MOFs) have emerged as particularly advantageous in this context owing to their unique structural and physicochemical characteristics. Their metal nodes exhibit catalytic and redox activity, while the exceptionally high surface area and porous architecture promote effective adsorption and interaction with target analytes. In addition, the tunable pore size and chemical functionality of MOFs enable tailoring of interfacial properties toward selective sensing

applications, positioning them as attractive platforms for advanced sensor design [32].

Despite these advantages, the intrinsically low electrical conductivity of pristine MOFs have constrained their direct use in electrochemical sensing, motivating the development of hybrid systems that integrate MOFs with conductive matrices. Such integration aims to improve electron-transfer kinetics, structural stability, and dispersion uniformity, ultimately enhancing sensor performance. For instance, Wang et al. reported a carbon paste electrode modified with a MIL-101(Cr)/reduced graphene oxide composite, where the large surface area of the MOF combined with the conductivity of rGO resulted in improved sensitivity and distinct peak separation for the simultaneous detection of catechol and hydroquinone [33]. Their one-pot hydrothermal incorporation strategy enabled partial in-situ reduction of graphene oxide and formation of a conductive porous composite, representing a practical innovation toward overcoming MOF conductivity limitations while maintaining facile electrode fabrication and reproducibility. Also materials such as graphite or multi-walled carbon nanotubes are preferred owing to their minimal toxicity, high electrical conductivity, and capacity to form uniformly dispersed, durable composites with MOF structures. As an illustration, Su et al. developed an electrochemical sensing platform based on an amine-functionalized Zr-MOF (UIO-66-NH_2) integrated with MWCNTs, exploiting the synergistic increase in surface area, reduced interfacial impedance, and enhanced electrocatalytic activity [34, 35]. This design enabled sensitive multi-analyte neurotransmitter detection and, notably, demonstrated real-time monitoring of dopamine release from living cells, highlighting the biocompatibility and translational potential of MOF–carbon nanocomposites for clinical diagnostics.

Collectively, these advancements highlight the increasing promise of electrochemical sensors incorporating MOFs for the selective and sensitive identification of molecules with biological and clinical significance, including dopamine. Both dopamine and phenylalanine are physiologically active substances with vital functions in nervous and metabolic physiology, commonly discussed in clinical and pharmacological contexts. As a primary neurotransmitter, dopamine participates in a wide array of bodily processes such as the regulation of mood, control of movement, reward signaling, and cognitive operations. In contrast, phenylalanine is an essential aromatic amino acid that serves as a precursor for tyrosine, which in turn is metabolized to L-DOPA and subsequently to dopamine and other catecholamine neurotransmitters. Beyond its role in neurotransmitter biosynthesis, phenylalanine is also critical for protein synthesis and contributes to maintaining normal growth, cognitive performance, and metabolic balance. [36, 37].

Given this metabolic relationship, monitoring dopamine in the presence of phenylalanine provides valuable insight into neurotransmitter homeostasis and metabolic balance. High or low levels of phenylalanine can directly affect dopamine biosynthesis, which in turn may contribute to neurological function and disorders such as Parkinson's disease, phenylketonuria, or other neuropsychiatric diseases [38]. Therefore, the development of analytical platforms capable of simultaneously resolving these metabolically linked species is of particular importance for advancing biochemical monitoring and clinical diagnostics.

Overcoming these obstacles necessitates the creation of electrochemical sensors with high selectivity and sensitivity. A particularly viable strategy involves modifying electrode surfaces with nanomaterials like metal-organic frameworks (MOFs). MOFs are characterized by their substantial surface area, adjustable pore dimensions, and metal centers capable of redox activity, which collectively improve molecular discrimination and charge transfer efficiency. Integration of such materials into carbon paste electrodes promotes distinct interactions with dopamine versus phenylalanine, allowing for improved resolution of their respective oxidation signals and a reduction in mutual interference [39-41]. Moreover, tailoring MOF composition and electrode architecture offers opportunities to engineer interfacial microenvironments that selectively favor target recognition, thereby addressing limitations associated with conventional unmodified electrodes.

Furthermore, electrodes functionalized with MOFs can leverage variations in the adsorption kinetics, surface binding affinity, and electrochemical reactivity of dopamine compared to phenylalanine [41]. This exploitation ultimately enhances the resolution between their

voltammetric peaks and allows for more precise quantitative analysis. Such a capability is especially beneficial in biological samples, where the presence of additional redox-active components and intricate background interferences can otherwise compromise the clarity of the analytical measurement [42]. Accordingly, incorporating MOF-based nanostructures into sensing platforms represents a rational step toward achieving reliable detection in complex matrices and lays the groundwork for the design strategy adopted in the present study.

The NH_2-MIL-88B metal–organic framework (MOF) exhibits a crystalline architecture composed of hexagonal channels and double-conical cages, providing a remarkably high specific surface area that is advantageous for electrochemical applications. Metal–organic frameworks are inherently structurally versatile; variations in precursor composition, stoichiometric ratios, and reaction conditions can yield distinct topologies, pore environments, and electronic properties. This synthetic tunability enables the rational selection of frameworks tailored to specific sensing objectives. In the present work, where enhancing sensor sensitivity through increased faradaic current response was a primary consideration, a framework capable of promoting efficient interfacial electron transfer was required [43, 44].

NH_2-MIL-88B(Fe) fulfills these criteria through its hybrid inorganic–organic architecture. The structure consists of Fe_3-oxo clusters coordinated by the linear ligand 2-aminoterephthalic acid (NH_2-H_2BDC). The aromatic backbone of the ligand contains conjugated π-systems that facilitate partial electron delocalization and promote charge mobility across the framework, while The presence of amine functional groups provides lone-pair electrons that increase the local electron density of the ligand framework and contribute to a higher density of electrochemically active sites within the structure, thereby promoting interfacial charge interaction and facilitating electron transfer processes. These interactions enhance adsorption affinity and improve interfacial charge transfer kinetics. Simultaneously, the Fe-oxo clusters serve as redox-active catalytic centers that mediate electron exchange processes, contributing to reduced charge-transfer resistance and increased oxidation current when incorporated into a conductive carbon matrix. The combined effects of conjugated pathways, electron-donating functional groups, and catalytically active metal sites therefore support improved electrochemical responsiveness and signal amplification [44, 45].

On this basis, NH_2-MIL-88B(Fe) was selected as an electrode modifier to strengthen current response and improve peak discrimination in voltammetric detection.

In summary, the concurrent and sensitive determination of dopamine and phenylalanine is important for clinical diagnostics, pharmacokinetic investigations, and neurochemical research. Accordingly, this study focuses on the development of a carbon paste electrode modified with NH_2-MIL-88B(Fe) for electrochemical quantification of dopamine and phenylalanine was systematically evaluated in phosphate buffer media as well as in human and pharmaceutical samples.

MATERIALS AND METHODS

Materials in use

All materials used in this study were of laboratory grade and applied without further purification. The following reagents were purchased from Merck: paraffin oil, graphite powder (99% purity), iron(III) chloride hexahydrate ($FeCl_3 \cdot 6H_2O$), 2-aminoterephthalic acid (NH_2-H_2BDC), N,N-dimethylformamide (DMF), sodium hydroxide (NaOH, 85%), phosphoric acid (H_3PO_4, 85%), and other high-purity chemicals. Dopamine and phenylalanine solutions at different concentrations were prepared by diluting a 0.01 M stock solution. Phosphate buffer solution (PBS) was used as the electrolyte, and buffer solutions with pH values ranging from 3.0 to 8.0 were obtained by adjusting with 0.1 M solutions of sodium hydroxide and phosphoric acid.

Analytical instruments

Electrochemical analyses were conducted using μ-Autolab TYPE III Potentiostat/Galvanostat in combination with a conventional three-electrode arrangement. The modified carbon paste served as the working electrode, a saturated Ag/AgCl electrode (KCl sat.) served as reference and a platinum wire were employed as the counter electrode. Different pH values of phosphate buffer solutions were prepared and adjusted using a Metrohm pH meter (Switzerland). A scanning electron microscopy (SEM, Mira3 Tescan) was used to characterize the morphology and X-ray diffraction (XRD, STOE diffractometer, Cu-Kα radiation) to investigate the crystalline structure

of the synthesized NH_2-MIL-88B(Fe).

Micro*wave assisted synthesis of modifier nanostructur*e

The metal–organic framework NH_2-MIL-88(Fe) was synthesized via a rapid microwave-assisted procedure. Iron(III) chloride hexahydrate ($FeCl_3 \cdot 6H_2O$) and 2-aminoterephthalic acid were dissolved in a 1:1 molar ratio in 30 mL of N,N-dimethylformamide (DMF) and sonicated for 10 min to obtain a clear yellow solution. The solution was transferred to a glass vessel and heated in a microwave reactor at 120 °C (140 W). During this process, the framework formed through a coordination-driven self-assembly mechanism. Partial hydrolysis of the hydrated Fe^{3+} precursor generated oxo/hydroxo intermediates, while thermal activation promoted deprotonation of the linker carboxylic groups. The resulting carboxylate anions coordinated to Fe^{3+} centers, inducing condensation into μ_3-oxo-bridged trinuclear iron clusters that served as secondary building units (SBUs). Subsequent bidentate coordination between linker carboxylates and neighboring Fe centers interconnected these SBUs, leading to nucleation and growth of the extended crystalline network. The microwave heating environment accelerated hydrolysis, coordination, and cluster organization, enabling rapid formation of the iron-based MOF structure. After cooling to room temperature, the resulting brown precipitate was collected by filtration, washed five times with ethanol to remove residual solvent and unreacted species, and dried overnight at 60 °C to obtain NH_2-MIL-88(Fe) [46, 47].

Method of preparation of working electrode

The working electrode, which was obtained by modifying carbon paste with NH_2-MIL-88(Fe), was obtained by mixing graphite powder (0.99 g) and nanostructure modifier (0.10 g) and adding paraffin oil to this homogeneous mixture at a weight ratio of 70:30. The resulting paste mixture was packed in a glass tube and connected to the rest of the electrical system with the help of a copper wire.

Processing of Real Samples

A volume of 1 mL freshly obtained human plasma or urine was diluted ten times using 0.1 M phosphate buffer solution (PBS, pH 7.0). For pharmaceutical analysis, a precisely weighed portion of a dopamine tablet was first dissolved in deionized water, after which PBS (pH 7.0) was added to adjust the solution to a final volume of 10 mL. Before electrochemical measurements, all sample solutions were passed through a 0.45 µm membrane filter to remove residual particulates.

RESULTS AND DISCUSSION

NH_2-MIL-88-B(Fe) characterization

Scanning electron microscopy (SEM) analysis was used to investigate the morphology and structural features of NH_2-MIL-88(Fe). The SEM images in Fig. 1a, b show that the material exhibits an octahedral geometry in its less developed crystals, while the more mature particles exhibit a distinct hexagonal shape similar to quartz.

The FT-IR spectrum of NH_2-MIL-88(Fe), presented in Fig. 1c, shows symmetric and asymmetric stretching vibrations of the $–NH_2$ group at around 3460 and 3370 cm^{-1}. Absorption bands corresponding to carboxylate groups are observed at 1580 and 1380 cm^{-1}. The peak at 1257 cm^{-1} is attributed to the C-N stretching in the aromatic ring, while the vibrations of the C-H bonds from the organic linkers appear near 766 cm^{-1}. In addition, characteristic O-Fe-O vibrational modes associated with Fe(III) coordination are evident at 521 and 412 cm^{-1} [48].

The XRD profile of NH_2-MIL-88(Fe), presented in Fig. 1d, displays well-defined diffraction peaks located at 2θ values of 9.1° (002), 10.3° (101), 13.1° (102), 16.6° (103), 18.7° (200), 19.4° (201), 20.7° (202), 26.3° (204), and 29.5° (302). These reflections correspond precisely to the simulated diffraction pattern generated from the crystallographic information file (CIF) of NH_2-MIL-88(Fe), archived in the Cambridge Crystallographic Data Centre (CCDC, ref. no. 647646) [49]. The strong agreement between experimental and simulated data provides clear evidence of the successful formation of NH_2-MIL-88(Fe) with excellent crystallinity and robust structural order [50].

Notably, the presence of intense peaks in the low-angle region is indicative of long-range periodic ordering, which is characteristic of porous metal–organic framework architectures and confirms the preservation of the framework topology. Furthermore, no sharp diffraction peaks are observed at higher diffraction angles (2θ > 30°), where crystalline iron oxide phases typically appear. The absence of such reflections suggests

that iron species are fully incorporated into the coordination framework rather than forming segregated oxide impurities such as Fe_2O_3.

Overall, the diffraction pattern confirms the formation of a phase-pure NH_2-MIL-88(Fe) structure with good crystallinity and structural integrity, supporting the successful synthesis of the targeted MOF material.[47, 48, 51].

Electrochemical Investigations

Differential pulse voltammetry (DPV) was employed to study the electrochemical oxidation

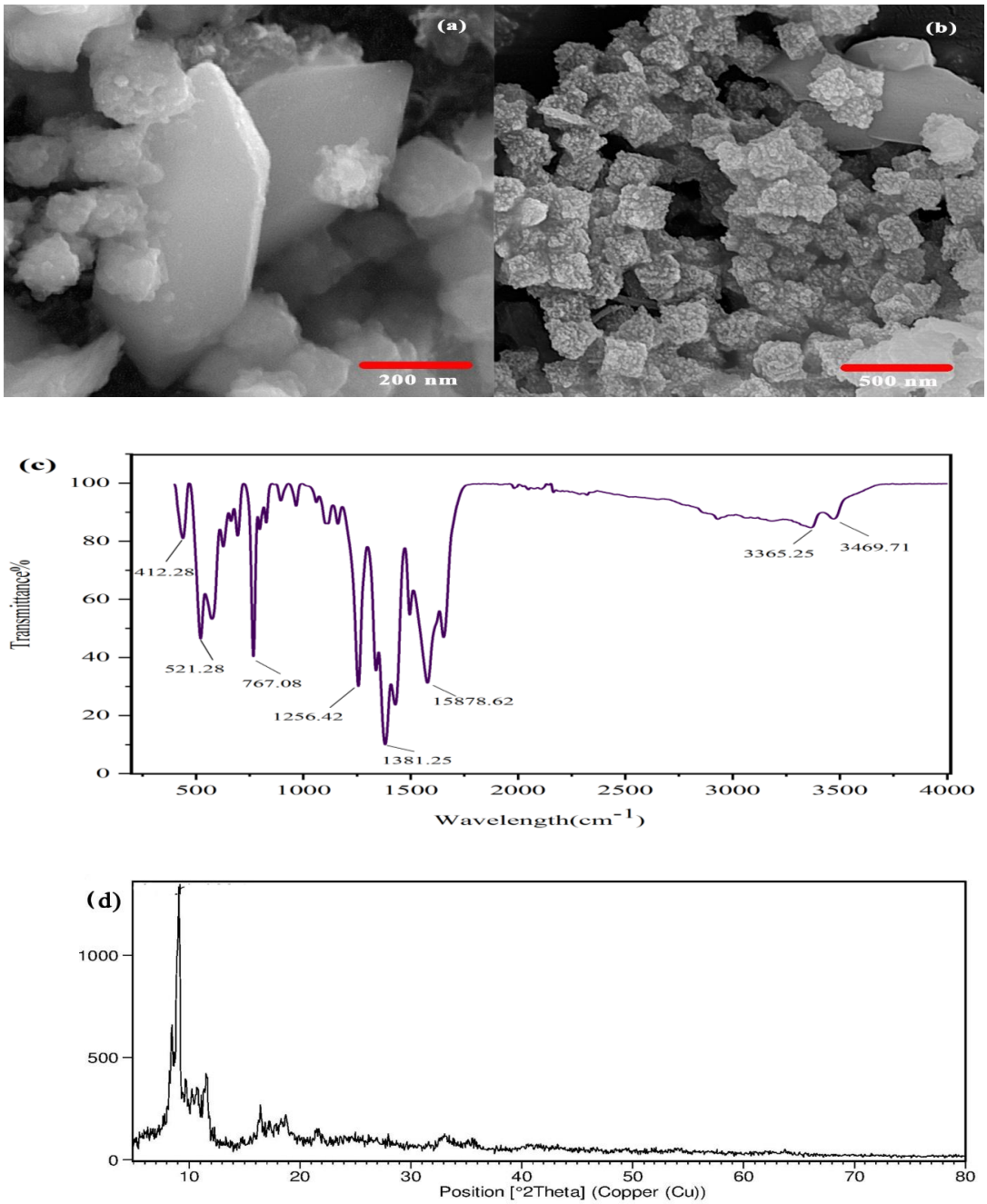

Fig. 1. The SEM micrographs (a,b), FT–IR analysis (c) and XRD pattern (d) of as-synthesized NH_2-MIL-88B(Fe).

of dopamine (500 µM) at the NH_2-MIL-88(Fe)/CPE modified electrode within the pH window of 3–8. As illustrated in Fig. 2a, the oxidation peak current (Ip) gradually increased as the pH rose from 3 to 7, attaining its maximum intensity at pH 7, after which a noticeable decline was observed at more

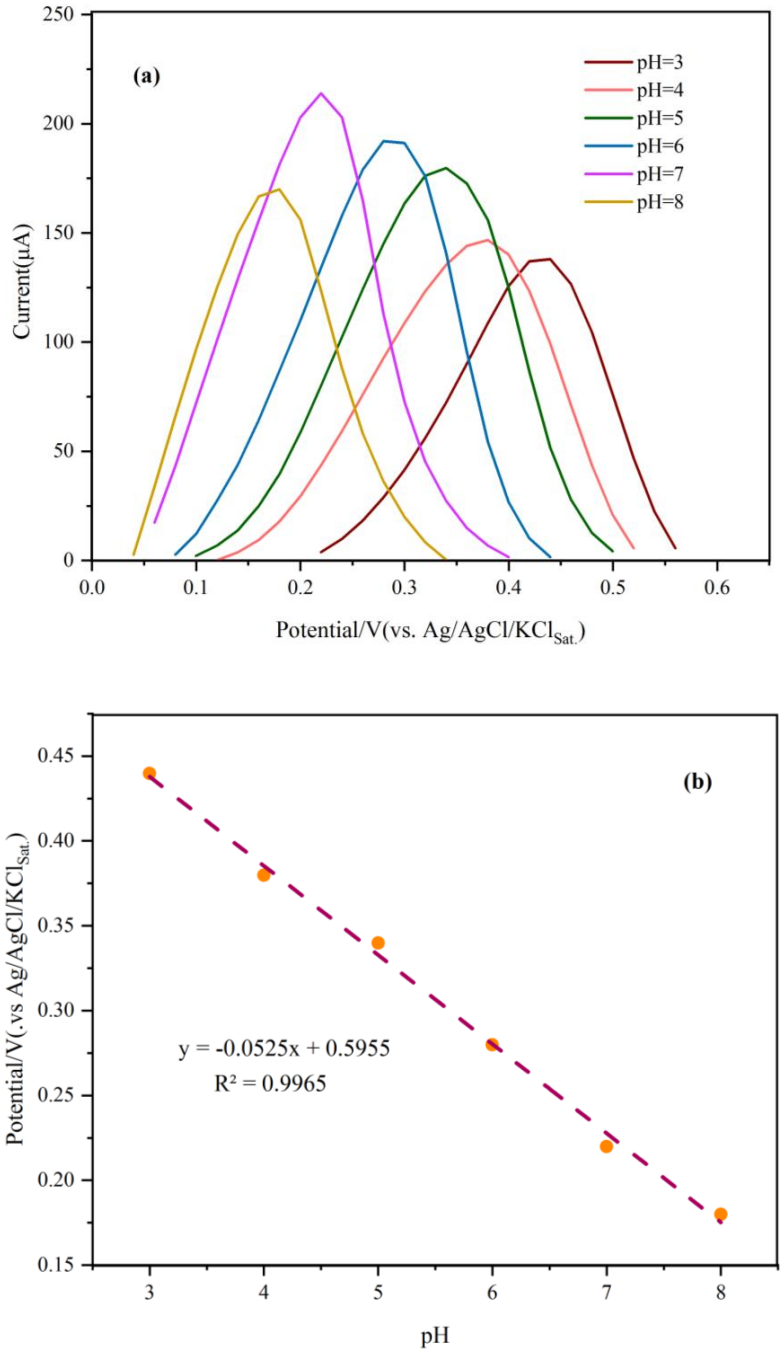

Fig. 2. The effect of pH on DPV of dopamine at a surface of the MOF/CPE (pH 3–8, respectively) (a) and E, vs. pH for the electrooxidation of 500 µM dopamine at a surface of the MOF/CPE (b).

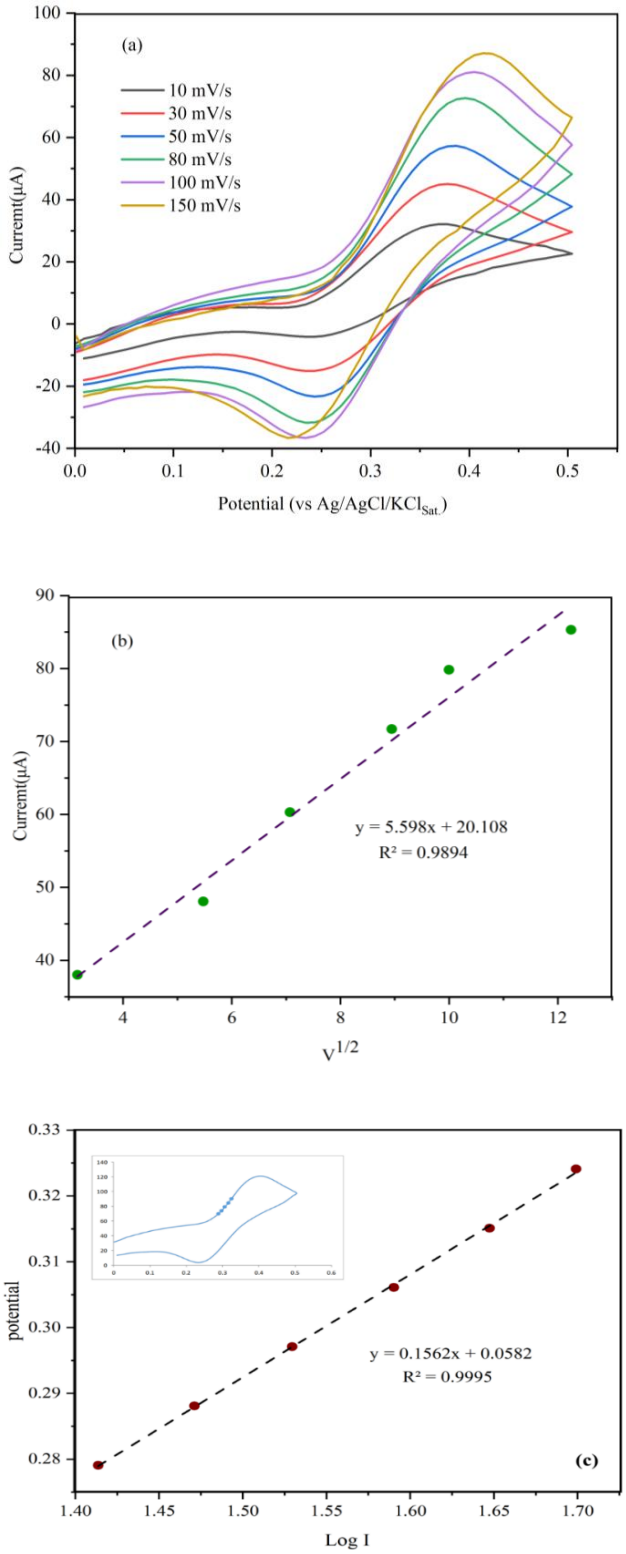

Fig. 3. (a) CV of dopamine by MOF/CPE at different scan rates (from inner to outer) of 10, 30, oxidation current in voltamogram of dopamine at MOF/CPE. (c) Tafel plot for dopamine by MOF/CPE with scan rate of 100.0 mV s^{-1} in the presence of 500 µM dopamine.

alkaline conditions. Based on this trend, pH 7 was selected as the most favorable environment for subsequent electrochemical investigations. In parallel, the oxidation peak potential (Ep) shifted progressively toward lower (more negative) values with increasing pH, signifying the active involvement of protons in the redox process. This observation highlights that the electrochemical response of dopamine is strongly dependent on the proton concentration at the electrode–solution interface. Fig. 2b further demonstrates a nearly perfect linear correlation between Ep and pH, with a slope of −0.0525 V/pH (R^2 = 0.9965). Such a slope is in close agreement with the theoretical prediction of the Nernst equation (E=E0-αRT/nF pH), thereby confirming a reaction pathway that involves the coupled transfer of one electron and one proton (n = 1) during dopamine oxidation.

The cyclic voltammetric profile obtained for a 500 µM dopamine solution prepared in 0.1 M phosphate buffer at pH (7.0) reveals a pronounced dependence of the anodic peak current on the applied scan rate. As the potential sweep was varied from 10 to 150 mV/s, a progressive enhancement in the peak current intensity was observed, shown in Fig. 3a. This behavior is in excellent agreement with the theoretical framework of the Randles–Sevcik equation, which predicts that the peak current (Ip) increases proportionally with the square root of the scan rate, reflecting accelerated electron transfer kinetics at the electrode surface under faster potential sweeps.

Fig. 3b,c provide further quantitative validation of this phenomenon. The plot of peak potential against the logarithm of current, as well as the linear relationship between current and the square root of scan rate, both demonstrate a strong correlation, thereby confirming that the electrochemical oxidation of dopamine at the NH_2-MIL-88(Fe)/CPE interface is predominantly governed by a diffusion-controlled mechanism. This indicates that the transport of dopamine molecules from the bulk solution to the electrode surface is the rate-determining step in the redox

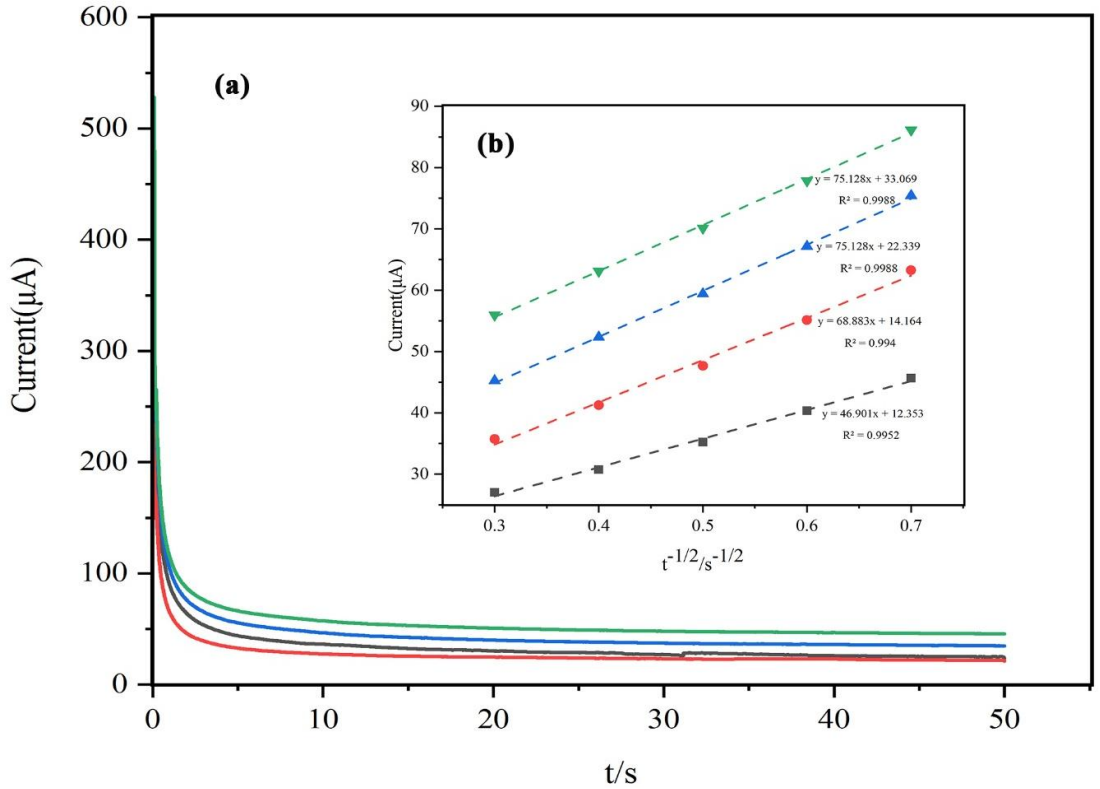

Fig. 4. (a) Chronoamperograms performed on MOF/CPE in the presence of 100, 200, 300 and 400 µM dopamine, from down to top, in PBS (pH 7.0), (b) Cottrell plots.

process.

In addition, the cyclic voltammograms exhibit a well-defined cathodic peak corresponding to the reduction of oxidized dopamine species. The presence of this return peak, combined with the absence of any significant negative shift in potential across the range of scan rates studied, provides compelling evidence for the reversible nature of the dopamine redox transformation. Such reversibility underscores the stability of the electron-proton transfer pathway and highlights the suitability of the modified electrode for sensitive and reproducible electrochemical detection of dopamine. Also, considering that the slope of the Linear plot in Fig. 3b is equal to (2.3RT/n (1-α) F) according to the Tafel plot, the electron transfer coefficient (α) was obtained to be about 0.8 (α = 0.8), which confirmed the existence of a reversible electrooxidation reaction.

Chronoamperometric measurements were performed over a concentration range of dopamine between 100 and 400 µM. The resulting current–time profiles displayed a clear linear dependence when plotted against the inverse square root of time ($t^{-1/2}$), a trend that is fully consistent with the theoretical prediction of the Cottrell equation. This agreement confirms that the electrochemical oxidation of dopamine under the applied conditions is predominantly governed by diffusion-controlled kinetics. From the slope of the calibration line, in combination with fundamental electrochemical parameters—including Faraday's constant (F = 96,485 $C \cdot mol^{-1}$), the single-electron transfer number (n = 1), and the defined electrode surface area (A = 0.115 cm^2) the diffusion coefficient of dopamine was calculated to be approximately 4.3 × 10^{-6} $cm^2 \cdot s^{-1}$, reflecting efficient mass transport within the system Fig. 4.

Fig. 5 illustrates the voltammetric behavior of both the unmodified carbon paste electrode (CPE) and the MOF-modified CPE when tested in a ferri/ferrocyanide redox system containing Fe(II)/

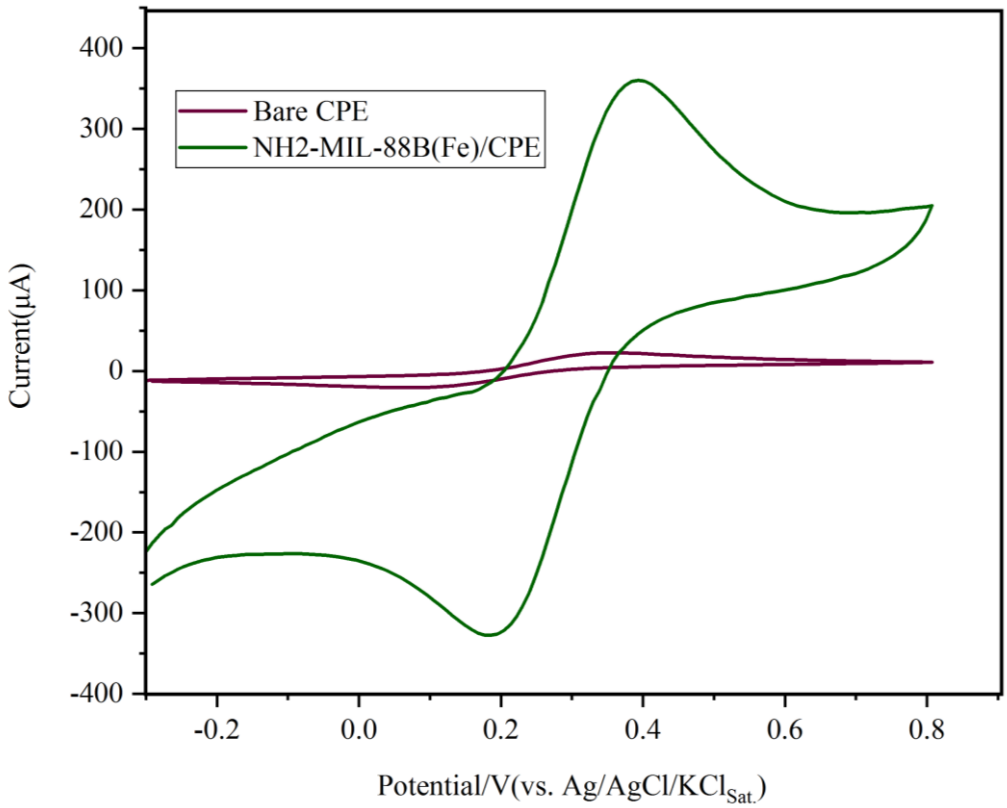

Fig. 5. Cyclic voltammetry of bare CPE and MOF/CPE electrodes in 5.0 mmol L^{-1} $[Fe(CN)_6]^{3-/4-}$ in 0.1 mol L^{-1} KCl

Fe(III) at a scan rate of 100 mV/s. The modified electrode produced a remarkably stronger current response than the bare CPE, highlighting its superior electrocatalytic efficiency. This enhancement can be attributed to the cooperative interaction between NH_2-MIL-88B(Fe) and graphite, which facilitates faster electron transfer and improves the overall performance of the sensor. To quantitatively assess this improvement, the electrochemically active surface area was estimated using the Randles–Sevcik equation based on cyclic voltammetric data obtained in 5 mM ferri/ferrocyanide solution. The calculated active surface area increased from 0.0106 cm² for the bare CPE to 0.115 cm² for the NH_2-MIL-88B(Fe)/CPE, corresponding to an approximately eleven-fold enhancement after modification. This substantial increase is attributed to the porous framework and high surface accessibility of NH_2-MIL-88B(Fe), which introduce abundant

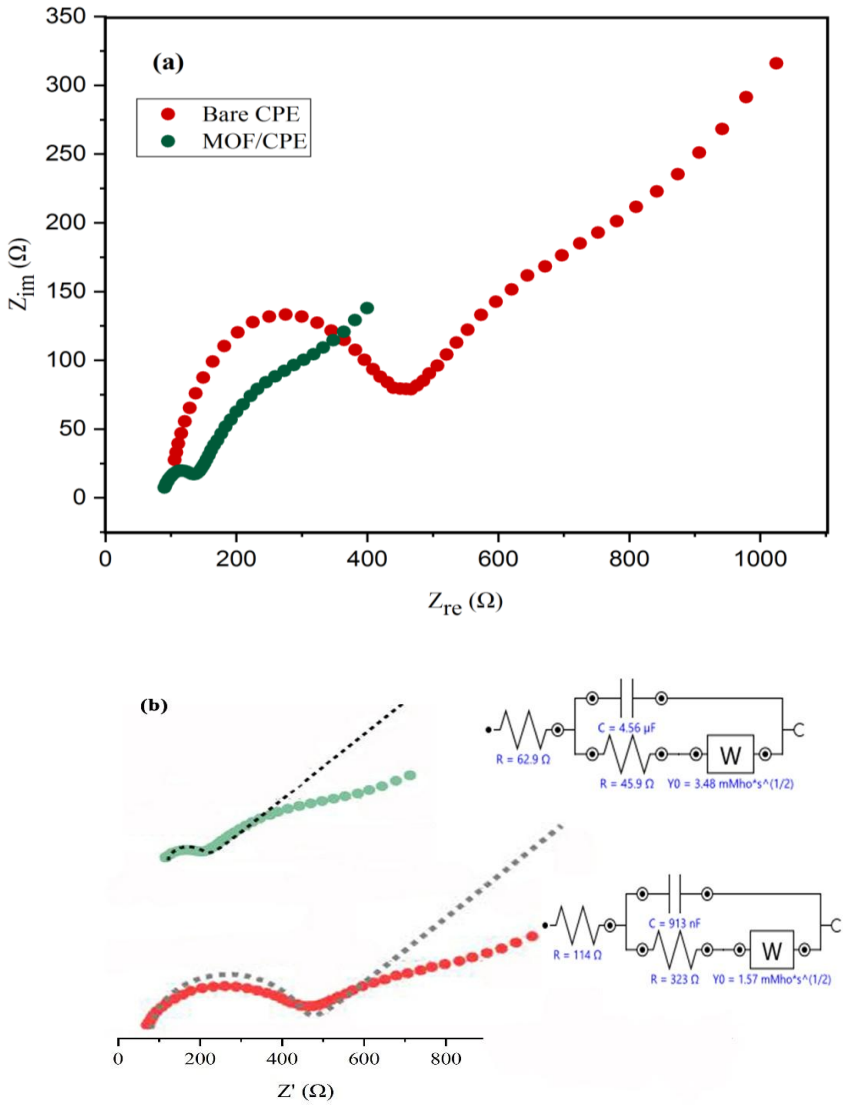

Fig. 6. (a) Nyquist diagrams of bare CPE and MOF/CPE electrodes in 5.0 mmol L^{-1} $[Fe(CN)_6]^{3-/4-}$ in 0.1 mol L^{-1} KCl, (b) Fitted Nyquist plots and their corresponding equivalent circuit for the bare and modified electrodes.

electroactive sites and facilitate electron transport at the electrode–electrolyte interface. Consequently, the cooperative contribution of the MOF structure and graphite matrix leads to improved electrocatalytic efficiency and overall sensor performance.

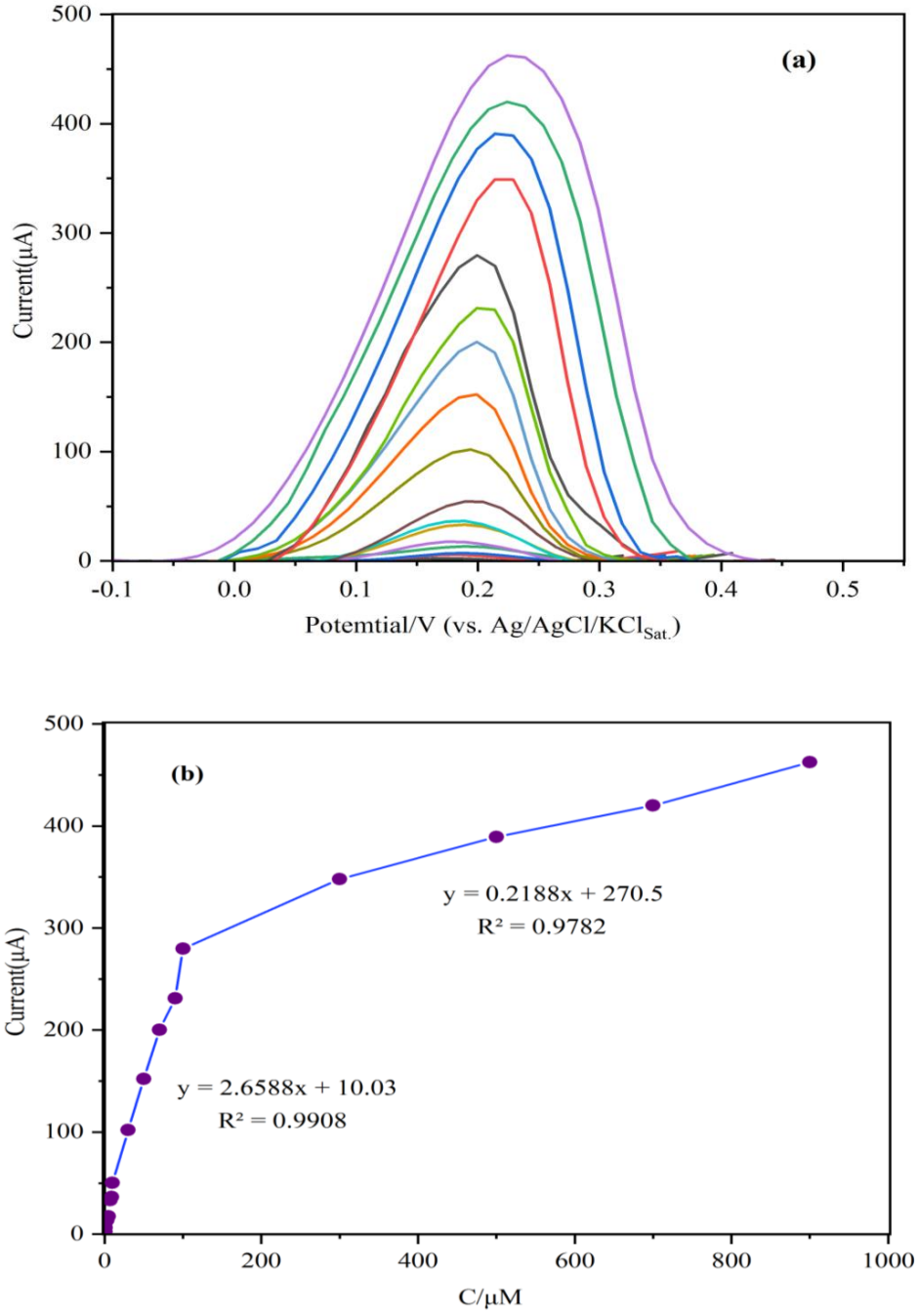

Fig. 7. (a) DPVs for various concentrations of dopamine (0.7, 1, 3, 5, 7, 10, 30, 50, 70, 90, 100, 300, 500, 700 and 900 μM) at surface of MOF/CPE at pH 7.0 and scan rate 100 mV s^{-1}. (b) Plots of linear range as a function of dopamine concentration.

To further elucidate the interfacial charge transfer characteristics, electrochemical impedance spectroscopy (EIS) was conducted using both the bare CPE and the MOF-modified CPE electrodes in a redox solution containing 5 mM $[Fe(CN)_6]^{3-/4-}$ with 0.1 M KCl as the supporting electrolyte. The Nyquist plots revealed a striking difference between the two electrodes Fig. 6a: the MOF/CPE exhibited a substantially smaller semicircular arc compared to the pristine CPE. This reduction in arc diameter corresponds to a lower charge transfer resistance (Rct), indicative of enhanced electrical conductivity and improved electron mobility at the electrode interface. The observed enhancement can be attributed to the nanostructured NH_2-MIL-88B(Fe) framework, which not only facilitates rapid electron transport but also increases the electrochemically active surface area (EASA), thereby amplifying the overall electrocatalytic performance of the modified sensor. As illustrated in Fig. 6b, the fitted Nyquist plots together with the corresponding equivalent circuit for both the bare and modified electrodes were obtained using NOVA 2.1 analytical software. The excellent agreement between the experimental data and the fitted curves confirms the reliability of the selected circuit model for describing the interfacial electrochemical behavior. From the fitting results, the charge-transfer resistance (Rct) values were extracted, revealing a pronounced decrease from 323 Ω for the bare electrode to 45.9 Ω after modification. This significant reduction indicates facilitated electron-transfer kinetics at the electrode–electrolyte interface, confirming the beneficial role of the NH_2-MIL-88B(Fe) modification in enhancing conductivity and electrochemical performance.

Concentration calibration curve

Fig. 7a illustrates the electrochemical performance of the fabricated MOF-modified electrode was systematically examined using differential pulse voltammetry (DPV) across a wide concentration window of dopamine ranging from 0.7 to 900 µM. As the analyte concentration increased, the anodic peak current exhibited a proportional enhancement, clearly defining two separate linear calibration domains that highlight the sensor's broad dynamic range and reliable quantitative response under varying experimental conditions Fig. 7b.

In addition, the detection capability of the system was rigorously evaluated. The calculated limit of detection (LOD) was found to be 0.18 µM, determined according to the conventional (3Sb/slope) criterion. This remarkably low threshold demonstrates the high sensitivity of the NH_2-MIL-88(Fe)/CPE platform and its ability to detect dopamine at trace levels with precision. Such performance underscores the synergistic contribution of the MOF structure in facilitating rapid electron transfer, expanding the

Table 1. Comparison of the obtained results with other reported works.

Nanocomposite	Electrode	Limit of detection (µM)	Linear range (µM)	Reference
DL-phenylalanine	GE	0.28	2-45	[52]
Tyrosinase/NiO	ITO/PET	1.38	2-100	[53]
Alumina/LC	CPE	0.6-0.4	0.13-65	[54]
Graphene	GCE	2.64	4-100	[55]
NH_2-MIL-88(Fe)	CPE	0.18	0.7-900	This work

Table 2. Interference investigatesd data for analysis of 500 µM dopaminae.

Species	Tolerant limits ($W_{substance}/W_{analyte}$)
Na^+, K^+, Ca^{2+}, NH_4^+, Mg^{2+}, Cl^-, I^-, SO_4^{2-}	500
NO_3^- , PO_4^{3-}, F^-, CO_3^{2-}	300
Glucose	600
Urea, and uric acid	300
Ascorbic acid	400
Albumin	500

electroactive surface area, and thereby enabling accurate quantification of dopamine even within complex biological or pharmaceutical matrices. A comparison of the results of this study with some other studies can be seen in Table 1.

Determination of dopamine in the presence of phenylalanine

The main goal of this work was to enable the simultaneous detection of dopamine alongside phenylalanine. DPV measurements revealed two very clear oxidation peaks at different potentials corresponding to each analyte, allowing their independent measurement. These distinct voltammetric responses confirm the electrode selectivity and peak resolution, which is characterized by the negligible signal shift of dopamine in the presence of different concentrations of phenylalanine, and it can be said that in the performance of the modified electrode NH_2-MIL-88(Fe)/CPE overlap and interference in the simultaneous detection and measurement of dopamine in the presence of phenylalanine have been minimized (Fig. 8).

Selectivity and stability investigations

Selectivity was evaluated by examining the sensor's response to dopamine in the presence of common biological interfering agents. The addition of glucose, urea, uric acid, ascorbic acid, albumin and ions caused no substantial alteration to the dopamine signal, demonstrating high selectivity (Table 2). Moreover, the sensor maintained more than 98% of its initial response after one month period, which confirms its long-term stability.

To measure the stability of the modified electrode performance, five cyclic voltammetry measurements were used consecutively in the presence of 500 µM dopamine in buffer medium with a scan rate of 100 mV/s. The results of this test showed that there was no significant change in the peak current, indicating the high stability

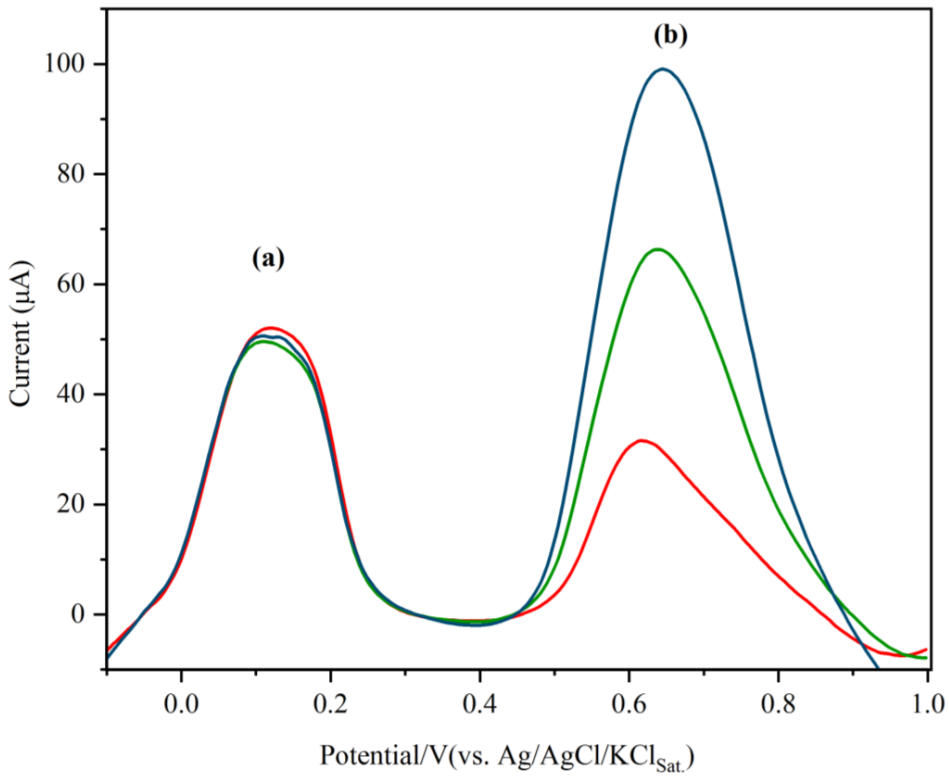

Fig. 8. DPV test of dopamine by NH_2-MIL-88(Fe)/CPE in the presence of different concentrations of phenylalanine 100, 300, and 500 µM (from bottom to top, respectively) in phosphate buffer pH 7. Peak (a) corresponds to dopamine and peak (b) corresponds to phenylalanine.

Table 3. Determination of dopamine in real samples.

Sample	Standard solution added(μM)	Signal (μA)	Recovery (%)	RSD
Human plasma	0	54.792*	------	------
	10	65.436	104.5	0.784
	15	77.528	97.6	1.053
	20	90.093	100.3	0.877
Human urine	0	52.131*	------	------
	10	64.918	101.8	1.13
	15	75.649	96.3	0.932
	20	89.25	100.1	0.889
Tablet	0	55.214	------	------
	10	66.826	100.8	0.541
	15	78.154	99.2	0.507
	20	89.907	100.02	0.990

*Sample containing an unknown amount of dopamine without adding dopamine standard solution

of the NH_2-MIL-88(Fe)/CPE electrode. Since the RSD in this measurement was less than 5%, it can be concluded that the working electrode has acceptable repeatability.

Real Sample Analysis

To validate its practical utility, the sensor was employed for dopamine detection in human serum via the standard addition technique. Given the complexity of this biological medium, a pretreatment step was applied to the samples prior to measurement. The obtained recovery values were accurate with negligible signal inhibition, proving that the MOF/CPE-based sensor can reliably quantify dopamine in intricate real-world matrices, including environments containing interferents such as phenylalanine (Table 3).

CONCLUSION

In this study, a carbon paste electrode integrated with a metal–organic framework (MOF) is reported for the first time as a highly sensitive platform capable of simultaneous determination of dopamine and phenylalanine. Comprehensive electrochemical characterization demonstrated that the incorporation of MOF into the carbon matrix markedly improves the intrinsic conductivity, enhances electrocatalytic efficiency, and expands the electroactive surface area of the electrode. These modifications collectively promote faster electron transfer kinetics, thereby enabling efficient detection of both target biomolecules.

Under carefully optimized experimental conditions, the engineered sensor delivers a broad linear response range from 0.7 to 100 μM and 100 to 900.0 μM, coupled with an exceptionally low detection threshold of 0.18 μM for dopamine. Kinetic analysis further revealed valuable parameters, including a transfer coefficient (α) of 0.8 and a diffusion coefficient (D) of 4.3×10^{-6} cm^2/s, in the electrochemical process. Importantly, validation experiments performed in real sample matrices confirmed the sensor's applicability, demonstrating reliable performance and practical utility for monitoring of dopamine and phenylalanine in complex environments.

CONFLICT OF INTEREST

The authors declare that there is no conflict of interests regarding the publication of this manuscript.

REFERENCES

1. Pognan F, Beilmann M, Boonen HCM, Czich A, Dear G, Hewitt P, et al. The evolving role of investigative toxicology in the pharmaceutical industry. Nature Reviews Drug Discovery. 2023;22(4):317-335.
2. Salamone JD, Correa M. The Neurobiology of Activational Aspects of Motivation: Exertion of Effort, Effort-Based Decision Making, and the Role of Dopamine. Annu Rev Psychol. 2024;75(1):1-32.
3. Seeman MV. History of the dopamine hypothesis of antipsychotic action. World Journal of Psychiatry. 2021;11(7):355-364.
4. Costa KM, Schoenbaum G. Dopamine. Curr Biol. 2022;32(15):R817-R824.
5. Franco R, Reyes-Resina I, Navarro G. Dopamine in Health and Disease: Much More Than a Neurotransmitter. Biomedicines. 2021;9(2):109.
6. Varma J, Maan KS, Mohiuddin S, Karnak F-U, Narang J, Shukla SK, et al. Development of Trp-AuNPs-rGO based

electrochemical active biosensing interface for dopamine detection. Chemical Physics Impact. 2024;9:100726.
7. Adam H, Gopinath SCB, Adam T, Salim ET, Fakhri MA. Dopamine Depletion in Parkinson's Disease and Therapeutic Options. CNS and Neurological Disorders - Drug Targets. 2025;24(8):577-581.
8. Minj A, Sahu S, Singh Tanwar LK, Ghosh KK. Au@ Ag nanoparticles: an analytical tool to study the effect of tyrosine on dopamine levels. RSC Advances. 2024;14(27):19271-19283.
9. Ferentzy A. No Ordinary Scribble: The Person Diagnosed with Schizophrenia Paints Their Soul. Culture, Medicine, and Psychiatry. 2024;48(3):655-662.
10. Selkoe DJ. The advent of Alzheimer treatments will change the trajectory of human aging. Nature Aging. 2024;4(4):453-463.
11. Gharai PK, Khan J, Pradhan K, Mallesh R, Garg S, Arshi MU, et al. Power of Dopamine: Multifunctional Compound Assisted Conversion of the Most Risk Factor into Therapeutics of Alzheimer's Disease. ACS Chem Neurosci. 2024;15(13):2470-2483.
12. Godino A, Salery M, Minier-Toribio AM, Patel V, Fullard JF, Kondev V, et al. Dopamine D1–D2 signalling in hippocampus arbitrates approach and avoidance. Nature. 2025;643(8071):448-457.
13. Parise EM, Nestler EJ. The neurobiological and molecular underpinnings of depressive phenotypes. APA handbook of depression: Classification, co-occurring conditions, and etiological processes (Vol. 1). American Psychological Association; 2026. p. 337-355.
14. Karki B, Trabelsi Y, Pal A, Taya SA, Yadav RB. Direct detection of dopamine using zinc oxide nanowire-based surface plasmon resonance sensor. Opt Mater. 2024;147:114555.
15. Khan R, Anjum S, Fatima N, Farooq N, Shaheen A, Fernandez Garcia J, et al. Development of Electrochemical and Colorimetric Biosensors for Detection of Dopamine. Chemosensors. 2024;12(7):126.
16. El Abbadi S, Elgamouz A, Kawde A-N, Douma M, El Moustansiri H, Tijani N. Fe3O4 nanoparticle-modified exfoliated carbon paste electrode for enhanced electrochemical detection of dopamine. Chemistry of Inorganic Materials. 2025;7:100125.
17. Buchmueller LC, Wunderle C, Laager R, Bernasconi L, Neyer PJ, Tribolet P, et al. Association of phenylalanine and tyrosine metabolism with mortality and response to nutritional support among patients at nutritional risk: a secondary analysis of the randomized clinical trial EFFORT. Frontiers in Nutrition. 2024;11.
18. Li S, Song H, Yu C. Causal association between phenylalanine and Parkinson's disease: a two-sample bidirectional mendelian randomization study. Frontiers in Genetics. 2024;15.
19. Akkaya H, SÜMer E. In Silico Approaches on Phenylalanine Hydroxylase Inhibitor-Related Compounds Used in Parkinson's Disease Treatment. Ankara Universitesi Eczacilik Fakultesi Dergisi. 2024;48(2):11-11.
20. Barker RA, Björklund A, Parmar M. The history and status of dopamine cell therapies for Parkinson's disease. Bioessays. 2024;46(12).
21. Correction to "Dopamine-Conjugated Extracellular Vesicles Induce Autophagy in Parkinson's Disease". Journal of Extracellular Vesicles. 2025;14(5).
22. Demailly A, Moreau C, Devos D. Effectiveness of Continuous Dopaminergic Therapies in Parkinson's Disease: A Review of L-DOPA Pharmacokinetics/Pharmacodynamics. Journal of Parkinson's Disease. 2024;14(5):925-939.
23. Yeni Y, Genc S, Ertugrul MS, Nadaroglu H, Gezer A, Mendil AS, et al. Neuroprotective effects of L-Dopa-modified zinc oxide nanoparticles on the rat model of 6-OHDA-induced Parkinson's disease. Sci Rep. 2024;14(1).
24. Muri R, Rummel C, McKinley R, Rebsamen M, Maissen-Abgottspon S, Kreis R, et al. Transient brain structure changes after high phenylalanine exposure in adults with phenylketonuria. Brain. 2024;147(11):3863-3873.
25. Shebl N, El-Jaafary S, Saeed AA, Elkafrawy P, El-Sayed A, Shamma S, et al. Metabolomic profiling reveals altered phenylalanine metabolism in Parkinson's disease in an Egyptian cohort. Frontiers in Molecular Biosciences. 2024;11.
26. Torres-Soto OI, Vega-Rios A, Dominguez RB, Osuna V. Electrochemical Detection of Dopamine with Graphene Oxide Carbon Dots Modified Electrodes. Chemosensors. 2025;13(1):7.
27. Biswas A, Lee S, Cencillo-Abad P, Karmakar M, Patel J, Soudi M, et al. Nanoplasmonic aptasensor for sensitive, selective, and real-time detection of dopamine from unprocessed whole blood. Science Advances. 2024;10(36).
28. Ait Lahcen A, Saidi K, Amine A. A critical review of electrosynthesized molecularly imprinted polymers in electrochemical sensing: Pros and cons. Current Opinion in Electrochemistry. 2025;54:101752.
29. Khamlichi RE, Bouchta D, Anouar EH, Atia MB, Attar A, Choukairi M, et al. A novel l-leucine modified Sol-Gel-Carbon electrode for simultaneous electrochemical detection of homovanillic acid, dopamine and uric acid in neuroblastoma diagnosis. Materials Science and Engineering: C. 2017;71:870-878.
30. Cernat A, Groza A, Tertis M, Feier B, Hosu-Stancioiu O, Cristea C. Where artificial intelligence stands in the development of electrochemical sensors for healthcare applications-A review. TrAC, Trends Anal Chem. 2024;181:117999.
31. Bhardwaj H, Archana, Noumani A, Himanshu JK, Chakravorty S, Solanki PR. Recent advancement in the detection of potential cancer biomarkers using the nanomaterial integrated electrochemical sensing technique: a detailed review. Materials Advances. 2024;5(2):475-503.
32. Khosropour H, Keramat M, Tasca F, Laiwattanapaisal W. A comprehensive review of the application of Zr-based metal–organic frameworks for electrochemical sensors and biosensors. Microchimica Acta. 2024;191(8).
33. Wang H, Hu Q, Meng Y, Jin Z, Fang Z, Fu Q, et al. Efficient detection of hazardous catechol and hydroquinone with MOF-rGO modified carbon paste electrode. J Hazard Mater. 2018;353:151-157.
34. Queiroz Felix AM, Alves Júnior S, da Silva Júnior AG, Cristiny Pereira M, Lima Oliveira MD, de Andrade CAS. Biosensor Based on Zif-8-90 5% Metal-organic Nanocomposite and Carbon Nanotubes Associated with Concanavalin a for Detection of Alpha-fetoprotein. Curr Anal Chem. 2024;20(7):516-525.
35. Su M, Peng W, Ding Z, Zhou Y, Gao H, Jiang Q, et al. Multi-walled carbon nanotubes-metal–organic framework nanocomposite based sensor for the monitoring of multiple monoamine neurotransmitters in living cells. Bioelectrochemistry. 2024;160:108776.
36. Lee DH, Lee W-Y. Enantioselective electrochemical L-phenylalanine sensor based on molecularly imprinted polymer embedded with redox probes. Microchem J. 2025;209:112641.
37. Fontana-Escartín A, Rosa E, Diaferia C, Lanzalaco S, Accardo

A, Alemán C. Evaluation of the electrochemical response of aromatic peptides for biodetection of dopamine. Journal of Colloid and Interface Science. 2025;679:441-454.
38. Zheng J, Zhang W, Miao Y-Y, Li X-R, Luo W-M, Yang X-L, et al. Interactive effect of phenylalanine with duration of diabetes on the risk of small vessel disease in Chinese patients with T2DM. Front Endocrinol (Lausanne). 2025;15.
39. Chinnasamy S, Mani A. Electrochemical stability and superior capacitance of bismuth cobalt metal-organic framework incorporated with vanadium disulfide nanosheet for supercapacitor application. J Alloys Compd. 2024;1002:175266.
40. Theyagarajan K, Kim Y-J. Metal Organic Frameworks Based Wearable and Point-of-Care Electrochemical Sensors for Healthcare Monitoring. Biosensors. 2024;14(10):492.
41. Wannassi J, Missaoui N, Mabrouk C, Castilla-Martinez CA, Moumen Y, Echouchene F, et al. A High-Performance Electrochemical Sensor Based on Ni–Pt Bimetallic Nanoparticles Doped Metal Organic Framework ZIF-8 for the Detection of Dopamine. ChemPlusChem. 2025;90(3).
42. Yang M, Xiao L, Chen W-T, Deng X, Hu G. Recent advances on metal-organic framework-based electrochemical sensors for determination of organic small molecules. Talanta. 2024;280:126744.
43. Zhou R, Liu L, Hu N, An Y. Improving adsorption and electron transfer capacities of Fe0 through NH2-MIL-88B confinement to boost electrochemical hydrodeoxygenation of nitrate. Chem Eng J. 2025;515:163975.
44. Tran LT, Dang HTM, Tran HV, Hoang GTL, Huynh CD. MIL-88B(Fe)-NH_2: an amine-functionalized metal–organic framework for application in a sensitive electrochemical sensor for Cd2+, Pb2+, and Cu2+ ion detection. RSC Advances. 2023;13(32):21861-21872.
45. Cooperative Design of the Ag3PO4/NH2MIL-88B (Fe/Co) Heterojunction Integrated with Conductive Polypyrrole for Advanced Photocatalytic Water Purification. American Chemical Society (ACS). http://dx.doi.org/10.1021/acsomega.3c09625.s001
46. Gao Q, Sheng Q, Zhang S, Tang Y. Recent trends on MIL-88(Fe) metal–organic frameworks: synthesis and applications in pollutant removal and detection. RSC Advances. 2025;15(32):26184-26200.
47. Shi L, Wang T, Zhang H, Chang K, Meng X, Liu H, et al. An Amine-Functionalized Iron(III) Metal–Organic Framework as Efficient Visible-Light Photocatalyst for Cr(VI) Reduction. Advanced Science. 2015;2(3).
48. Royan F, Abbasi A, Hosseini M-S, Ghorbani P. Enhanced cationic dye removal from water media via electrostatic interaction-assisted incorporation of phosphotungstic acid into NH_2-MIL-88B(Fe) through the breathing effect. Colloids Surf Physicochem Eng Aspects. 2025;708:135977.
49. Liu J, Yang J, An S, Wen M, Wang X, Gong R, et al. Synthesis and electromagnetic properties of NH2-MIL-88B(Fe) crystals with morphology and size controllable through synergistic effects of surfactant and water. Journal of Materials Science: Materials in Electronics. 2022;33(17):14228-14239.
50. Pham M-H, Vuong G-T, Vu A-T, Do T-O. Novel Route to Size-Controlled Fe–MIL-88B–NH2 Metal–Organic Framework Nanocrystals. Langmuir. 2011;27(24):15261-15267.
51. Zango ZU, Abu Bakar NHH, Sambudi NS, Jumbri K, Abdullah NAF, Kadir EA, et al. Adsorption of chrysene in aqueous solution onto MIL-88(Fe) and NH2-MIL-88(Fe) metal-organic frameworks: Kinetics, isotherms, thermodynamics and docking simulation studies. Journal of Environmental Chemical Engineering. 2020;8(2):103544.
52. Hareesha N, Manjunatha JG. Fast and enhanced electrochemical sensing of dopamine at cost-effective poly(DL-phenylalanine) based graphite electrode. J Electroanal Chem. 2020;878:114533.
53. Roychoudhury A, Basu S, Jha SK. Dopamine biosensor based on surface functionalized nanostructured nickel oxide platform. Biosensors and Bioelectronics. 2016;84:72-81.
54. Plotsky PM, Gibbs DM, Neill JD. Liquid Chromatographic-Electrochemical Measurement of Dopamine in Hypophysial Stalk Blood of Rats*. Endocrinology. 1978;102(6):1887-1894.
55. Kim Y-R, Bong S, Kang Y-J, Yang Y, Mahajan RK, Kim JS, et al. Electrochemical detection of dopamine in the presence of ascorbic acid using graphene modified electrodes. Biosensors and Bioelectronics. 2010;25(10):2366-2369.